SUPPLEMENTAL MATERIAL

Supplemental Methods

Monocrotaline, SU5416, Chronic Hypoxia or SU5416 and Chronic Hypoxia Models of PH.

Female or male *Bmpr2* mutant rats were randomly assigned to control or treatment groups. PH was induced in rats, at the age of 4-6 week, with a single subcutaneous dose of monocrotaline (60mg/kg) or SU5416 (20mg/kg). Control groups received a single subcutaneous injection of DMSO. Alternatively, rats with or without an injection of SU5416 (20mg/kg) were exposed to hypoxia (10% O_2) in an airtight plexiglass hypoxia chamber with simulated O_2 controller (Biospherix). Rats maintained in normoxic conditions (20% O_2) served as controls. All animals were euthanized at post-treatment week 3.

Measurements of Hemodynamics

Rats were anesthetized with ketamine hydrochloride (70 mg/kg), and xylazine (10 mg/kg) injected i.p. prior to right heart catheterization. Right ventricular systolic pressure (RVSP) measurements were obtained by insertion of a Micro Tip pressure transducer (model SPR-671, 1.4F; Millar Instruments) through the jugular vein into the RV. Signals were recorded continuously with a TC-510 pressure control unit 236927/R17 (Millar Instruments) coupled to a Bridge Amp (AD Instruments). Data was collected with the Powerlab 4/30 data acquisition system (AD Instruments) and analyzed with Chart Pro software (AD Instruments). RV was dissected from left ventricle (LV), and septum (S) and each was weighed. Fulton index of RV/(LV+S) was calculated to determine the degree of right ventricular hypertrophy (RVH). All quantification was performed in a blinded fashion.

Degree of Muscularization

To determine the degree of muscularization, vessels <100 μm with positive α-SMA cell staining surrounding endothelial cells were identified and classified as: none, partially or fully muscularized. The degree of muscularization was expressed as % ratio of number of vessels to the number of total vessels. All quantification was performed in a blinded fashion.

Echocardiography

Echocardiographic evaluation of right ventricular dimensions and pulmonary hemodynamics were performed using the Vivid 7 Dimension Cardiovascular Imaging System (GE), equipped with a 14 MHz transducer. Rats were lightly sedated with isoflurane for the duration of the procedure. The chests were depilated prior to obtaining images. Rats were laid supine on a warming-handling platform. Pulmonary artery Doppler tracings were obtained from the pulmonary artery parasternal short-axis views. RV free wall was imaged from a modified parasternal long-axis view. All measurements were made in the expiratory phase of the respiratory cycle.

Western Blotting

Protein samples were separated by sodium dodecyl sulfate-polyacrylamide gel electrophoresis on 4% to 12% Bis-Tris gradient gels (Life Technologies), transferred onto nitrocellulose membranes (Bio-Rad), and incubated with primary antibodies: mouse anti-BMPR2 (1:2 000, Abcam), rabbit anti-p-SMAD1/5/9 (1:500,

Cell Signaling), rabbit anti-SMAD1 (1:1000, Cell Signaling), rabbit anti-Id1 (1:500, Abcam), rabbit anti-α-SMA (1:500, Sigma-Aldrich), rabbit anti-5-LO (1:1000, Cell Signaling), rabbit anti-p-SMAD 2/3 (1:500, Cell Signaling), rabbit anti-SMAD2 (1:1000, Cell Signaling), rabbit anti-p-p38 (1:2000, Cell Signaling), rabbit anti-p38 (1:2000, Cell Signaling) or mouse anti-β-actin (Sigma-Aldrich). Western blots were quantified using densitometry analysis by the ImageJ software.

Immunofluorescent Staining of Tissue Sections from *Bmpr2* Mutant Rats or PAECs.

Frozen sections were incubated with antibodies against rabbit- or mouse-von Willebrand Factor (1:100, Abcam), rabbit anti-cleaved Caspase3 (1:50, Cell Signaling)rabbit or mouse anti-α-SMA (1:200, Abcam), rabbit anti-Ki67 (1:50, Abcam), rabbit anti-5-LO (1:50, Cell Signaling), rabbit anti-p-SMAD 2/3 (1:50, Cell Signaling), rabbit anti-p-STAT3 (1:50, Cell Signaling), rabbit anti-GFP(1:50, Abcam) or mouse anti-CD68 (1:50, BD). PAECs were cultured in chamber slides, fixed in 4% paraformaldehyde, and permeabilized by 0.1% Triton X-100. Slides were incubated with primary antibodies against rabbit anti-5-LO (1:25, Cell Signaling) or VE-cadherin (1:50, Abcam). Negative controls stained with isotype IgG were run in parallel. Fluorescent-tagged secondary antibodies were used at 1:400 (Life Technologies). All slides were mounted using Vector Shield with DAPI to stain nuclei (Vector Laboratories). Images were acquired by Zeiss 800 confocal microscopy and analyzed using ImageJ software.

Morphometric Measurements.

Percentage of co-staining of vWF/α-SMA or 5-LO/vWF/α-SMA was calculated as area density. Numbers of $Ki67^+$, p-$SMAD2/3^+$ or p-$STAT3^+$ cells were quantified based on at least six high power fields per sample. For quantification of VE-cadherin junctions, junctional length was calculated by measuring the length of all segments of continuous and discontinuous junctions on confluent ECs stained for VE-cadherin. The sum of all segments was considered the total junctional length (100%), and the sum of all discontinuous segments was calculated as the percentage of total junctional length. A minimum of six fields was quantified (≈30 cells per field) per experiment. All measurements were performed using ImageJ Software on immunofluorescent confocal images.

Quantitative Reverse-Transcription PCR(qPCR)

Total RNA was extracted and purified from cells or tissues using the RNA MiniPrep Kit (Qiagen). The quantity and quality of RNA were determined using a Nanodrop (Thermo Fisher). RNA was reverse transcribed to cDNA using the High Capacity RNA to cDNA Kit (Applied Biosystems) according to the manufacturer's instructions. Quantitative PCR (qRT-PCR) was performed using FastStart SYBR Green (Roche) on a Lightcycler 480. mRNA expression relative to GAPDH mRNA levels were calculated using the delta-delta threshold cycle ($\Delta\Delta CT$) method. Primers, designed using National Center for Biotechnology Information's Primer-BLAST function, are shown in the Supplemental Table 1. Inflammatory Response

and Autoimmunity RT^2 Profiler PCR arrays were purchased from Qiagen: Rat (330231, PARN-077Z) and Human (330231, PAHS-077Z).

Patients

Human hPAH specimens were obtained following lung transplantation. Control subject tissue was collected during lobectomy or pneumonectomy for localized lung cancer; pulmonary arteries were studied at a distance from the tumor areas. Transthoracic echocardiography was performed preoperatively in the control cohort to rule out PAH. All human studied were approved by the French Network on Pulmonary Hypertension and had given written informed consent by the patients (Protocol N8CO-08- 003, ID RCB: 2008-A00485-50, approved on June 18, 2008). Demographic and clinical data relevant to hPAH patients and controls are provided in Supplemental Table 2 and 3.

Immunofluorescent Staining of Human Tissue.

Paraffin-embedded formalin-fixed human lung tissue from 11 control subjects and 19 fPAH patients was studied and compared. Antigen retrieval was performed by steaming the slides for 20 minutes in 0.01M citrate buffer, pH 6.0 and then blocking with 1% normal donkey serum in PBS for 15 minutes. Slides were incubated with rabbit anti-5-LO (1:25, Cell Signaling) and mouse anti-von Willebrand Factor (1:50, Abcam) in 1% donkey serum overnight at 4°C, followed by corresponding secondary antibodies (1:400, Invitrogen). Negative controls with isotype IgG were run in parallel. Images were acquired by Zeiss 800 confocal microscopy and analyzed with ImageJ.

Human Primary Cell Culture

PAECs were predominantly harvested from small pulmonary arterials (<1 mm) from explanted lung of one hPAH patient obtained at the time of transplantation, and from one donor control lung, via the Pulmonary Hypertension Breakthrough Initiative Network, funded by the Cardiovascular Medical and Education Fund and NHLBI. Human control PAECs were infected with lentiviral sh*Bmpr2* to mimic BMPR2 signaling loss. Cells were cultured with 400nM LTB_4 in the serum free endothelial cell medium supplied with endothelial-specific growth factors for 1, 3, 5 or 7 days to assess the effects of increased 5-LO-mediated inflammation. Serum free conditions were used as a general approach in eicosanoid biology to preserve the bioactivity of LTB_4.

Lentivirus-based RNAi

Lentiviral transduction particles expressing specific shRNA sequence in MISSION® pLKO.1-CMV-tGFP vector was purchased from Sigma-Aldrich. Two clones (NM_001204.5-3321s1c1 and NM_001204.x-3537s1c1) were tested for efficiency in silencing *Bmpr2*. Two clones (NM_181657.3-2522s21c1 and NM_181657.3-2961s21c1) were tested for efficiency in silencing *Ltb4r1*. Clone ID NM_004612.2-5651s1c1 and NM_005902.3-1218s21c1 was used to target *Tgfbr1* or *Smad3*, respectively. Viral particles containing shRNA sequence targeting *tGFP* were used as control in all experiments. Gene expression after knockdown was quantified by western blot or qRT-PCR.

Flow Cytometry Analysis
PAECs were fixed, permeablized and stained with FITC-labeled Ki67 (Invitrogen), APC-Cy7-labeled cleaved Caspase 3 (Invitrogen) or APC-labeled α-SMA (Invitrogen). Propidium iodide was used to exclude the dead cell population. Flow cytometry used LSRFortessa cell analyzer (BD Biosciences).

Quantification of VE-cadherin Junctions
Junctional length was calculated by measuring the length of all segments of continuous and discontinuous junctions on PAECs stained for VE-cadherin. The sum of all segments was considered the total junctional length (100%), and the sum of all discontinuous segments was calculated as the percentage of total junctional length. A minimum of 5 fields was quantified (≈30 cells per field) per experiment.

RNAseq Analysis of PAECs
PAECs, at passage number 3–5 from a control donor, were infected by lentivirus expressing sh*Bmpr2* to silent BMPR2 signaling. These cell were subsequntially cultured with Ad*Gfp* vector or Ad*Alox5* for 7 days. Three replicates were performed for each treatment group.Total RNA was extracted using the RNeasy Mini Kit (QIAGEN). Lentiviral knockout effiency of *Bmpr2* was confirmed by RT-PCT. Libraries were prepared using the TruSeq Stranded Total RNA Library Prep Kit (Illumina) and subjected to sequencing on 1–2 Illumina HiSeq 4000 lanes to obtain an average of approximately 100-150 million uniquely mapped reads for each sample (Stanford Genomics and Personalized Medicine Sequencing Facility). Differential gene expression analysis was performed in R using EBSeq package, an empirical Bayes hierarchical model for inference in RNAseq experiments, using false discovery rate (FDR) of 0.05 to retrieve list of differentially expressed genes (DEGs). Differentially expressed genes were ranked by posterior fold change and enriched for gene sets using The Molecular Signatures Database (MSigDB) and Gene Set Enrichment Analysis (GSEA) tools developed by the Broad Institute. Transcriptome data (FASTQ files) have been submitted to the Gene Expression Omnibus (GEO, http://www.ncbi.nlm.nih.gov/geo/), an international public repository for genomic data sets (Barrett et al., *Nucleic Acids Res*. 2013 Jan; 41(Database issue): D991–D995.); the accession number for the RNAseq data in this study is GSE133749.

TGF-β/SMAD2/3 Reporter Assay
TGF-β activities used pGL4.48 [*luc2p*/SBE/Hydro] vector (Promega) to measure the SBE (SMAD binding element)-mediated transcriptional of luciferase reporter gene *luc2P*. Briefly, PAECs were seeded in the 96-well plate at the density of $3.0x10^4$ cell/well 1 day before transfection. Cells were transfected with the pGL4.48 [*luc2p*/SBE/Hydro] vectors for 18hrs and then subjected to assays using ONE-GloTM Luciferase kit (Promega) following the manufacturer's technical manual.

Supplemental Table 1. PCR Primer Sequence

Gene(human)	Primers
Ilr1r1	F- GTGCTTTGGTACAGGGATTCCTG R- CACAGTCAGAGGTAGACCCTTC
Il6r	F- GACTGTGCACTTGCTGGTGGAT R- ACTTCCTCACCAAGAGCACAGC
Gp130	F- CACCCTGTATCACAGACTGGCA R- TTCAGGGCTTCCTGGTCCATCA
Tlr2	F- CTTCACTCAGGAGCAGCAAGCA R- ACACCAGTGCTGTCCTGTGACA
Tlr4	F- CCCTGAGGCATTTAGGCAGCTA R- AGGTAGAGAGGTGGCTTAGGCT
Gm-cfs	F- GGAGCATGTGAATGCCATCCAG R- CTGGAGGTCAAACATTTCTGAGA
Pai-1	F- GGCTGACTTCACGAGTCTTTCA R- TTCACTTTCTGCAGCGCCT
Tgfβ1	F- TACCTGAACCCGTGTTGCTCTC R- GTTGCTGAGGTATCGCCAGGAA
Itga9	F- CCTCTGACACCAGTTCTCCGC R- GCCTCGAAGACCACCGTCA
Slug	F- GCTGGTAGGGAGTCAGAAGGA R- TGGTGGTTTTCCGGGTCTTG
Snail	F- CGAACTGGACACACATACAGTG R- CTGAGGATCTCTGGTTGTGGT
Calponin	F-CTGTCAGCCGAGGTTAAGAAC R- GAGGCCGTCCATGAAGTTGTT
Ve-cadherin	F- TTGGAACCAGATGCACATTGAT R- TCTTGCGACTCACGCTTGAC

Supplemental Table 2. Control Patients Demographics

Age	Sex	Cause of Death
65	M	Adenocarcinoma
69	F	Squamous cell cardinoma
40	M	Carcinoid tumor
43	M	Adenocarcinoma
55	F	Adenocarcinoma
48	F	Squamous cell cardinoma
36	M	Adenocarcinoma
55	F	Leimyoma
60	M	Adenocarcinoma

Supplemental Table 3. *Bmpr2* Mutant fPAH Patients Demographics

Age	Sex	Localization of bmpr2 mutation	Amino Acid Change
52	M	exon 11, kinase domain	Arg491Trp
46	M	exon 6, kinase domain	Arg221X
45	F	exon 6, kinase domain	Arg221X
55	M	exon 7, kinase domain	Ser301Pro
19	F	exon 8, kinase domain	Arg332X
43	F	exon 6, kinase domain	large rearrangement
49	F	exon 7, kinase domain	Ser301Pro
19	M	exon 11, kinase domain	Arg491Trp
21	M	exon 6, kinase domain	Lie261serfsX4
52	F	exon 7, kinase domain	Arg321X
43	F	exon 1, ligand binding domain	Trp16X
49	F	exon 12, cytoplasmic domain	Arg873X
55	M	exon 5	His184ArgfsX8
26	M	exon 3, ligand binding domain	Cys94Gly
56	F	exon 3, ligand binding domain	Asn124Asp
40	F	intron 7, kinase domain	Splice defect
25	M	intron 3	Splice defect

Supplemental Figure 1

Generation of the *Bmpr2*$^{+/\Delta 527bp}$ and the *Bmpr2*$^{+/\Delta 16bp}$ rats using Zinc Finger Nuclease technology

Wild type

***Bmpr2*$^{+/\Delta 527bp}$**

ctg tcc tcc gag t~~cg gga gcg atg cga ... ccc ttt cgg gtg c~~ccc tgg ctg tta tgg gcc gtg ctg
ctg gtc agc act acg gct ggt

Δ527bp

***Bmpr2*$^{+/\Delta 16bp}$**

gat act tcc tcg ctg cag c~~gg ccc ttt cgg gtg cc~~c tgg ctc tta tgg gcg

Δ16bp

Supplemental Figure 2

Ad*Alox5* induces severe PAH in the *Bmpr2*$^{+/\Delta 527bp}$ rats

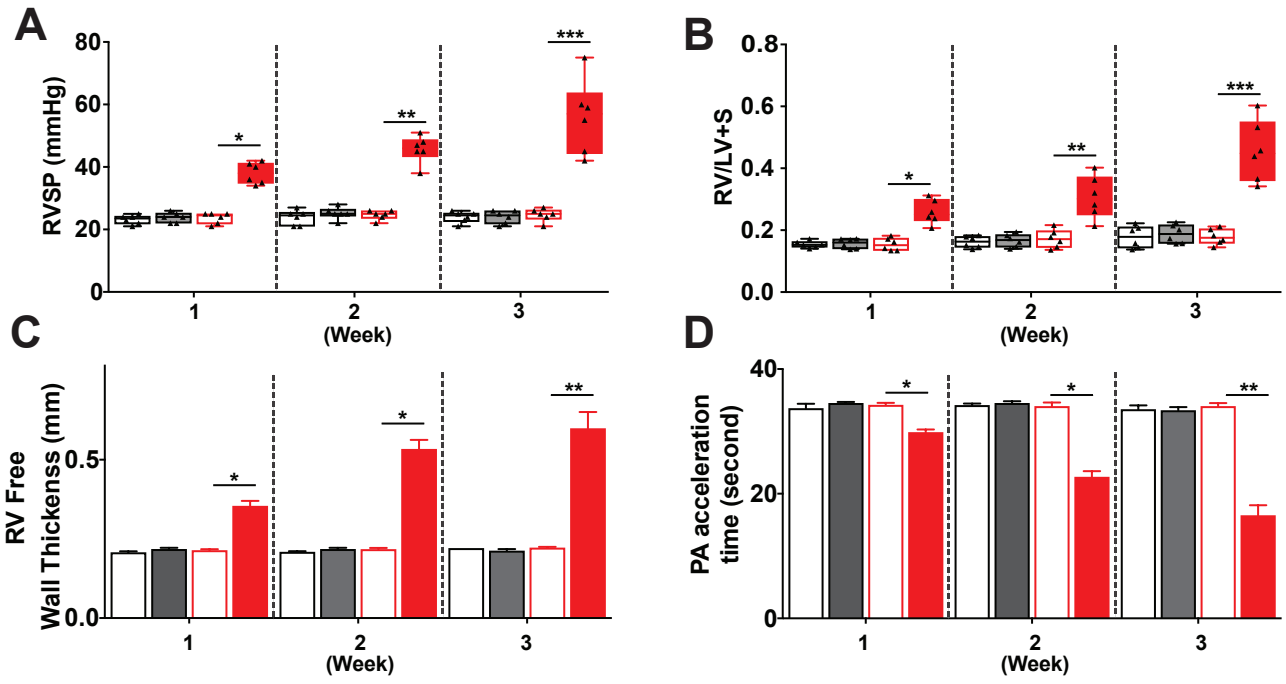

E

	Bmpr2$^{+/\Delta 527bp}$(week 3)		P value
	Ad*GFP*	Ad*Alox5*	
n	4	4	-
Heart Rate(bpm)	391.25±12.57	309.98±8.12	*
LVESP(mmHg)	102.3±1.7	94.35±4.7	ns
LVEDP(mmHg)	6.68±0.5	7.5±0.4	ns
Stroke Volume(RVU)	24.08±4.1	20.02±1.5	ns
Cardiac Output(RVU/min)	7926.32±227	8018.65±242	ns
dP/dt max (mmHg/s)	8214.83±132	8056.74±205	ns

Legends for A, B, C, D, G and I

- WT *(AdGFP)*
- WT *(AdAlox5)*
- *Bmpr2*$^{+/\Delta 527bp}$ *(AdGFP)*
- *Bmpr2*$^{+/\Delta 527bp}$*(AdAlox5)*

Supplemental Figure 3

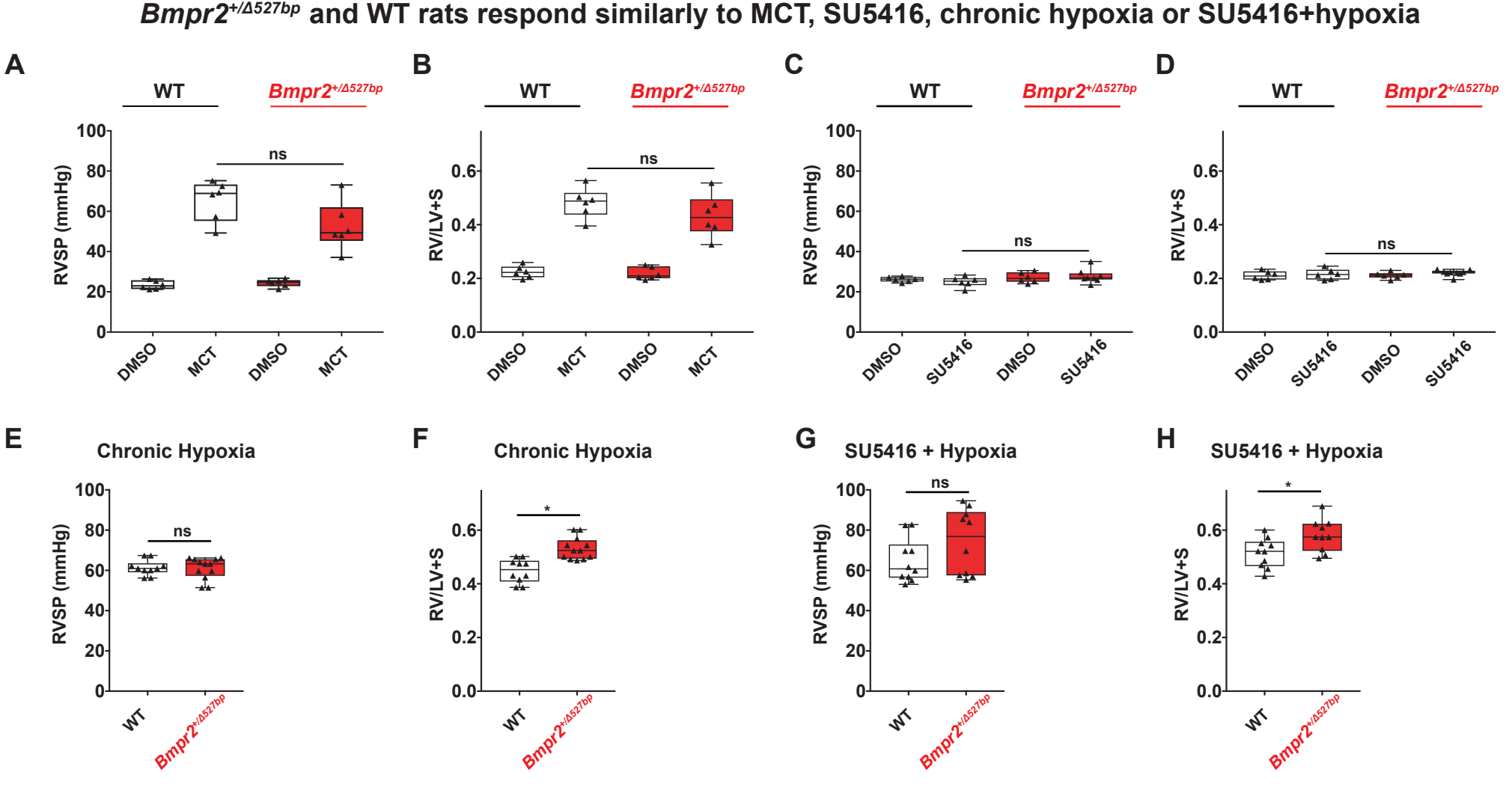

Supplemental Figure 4

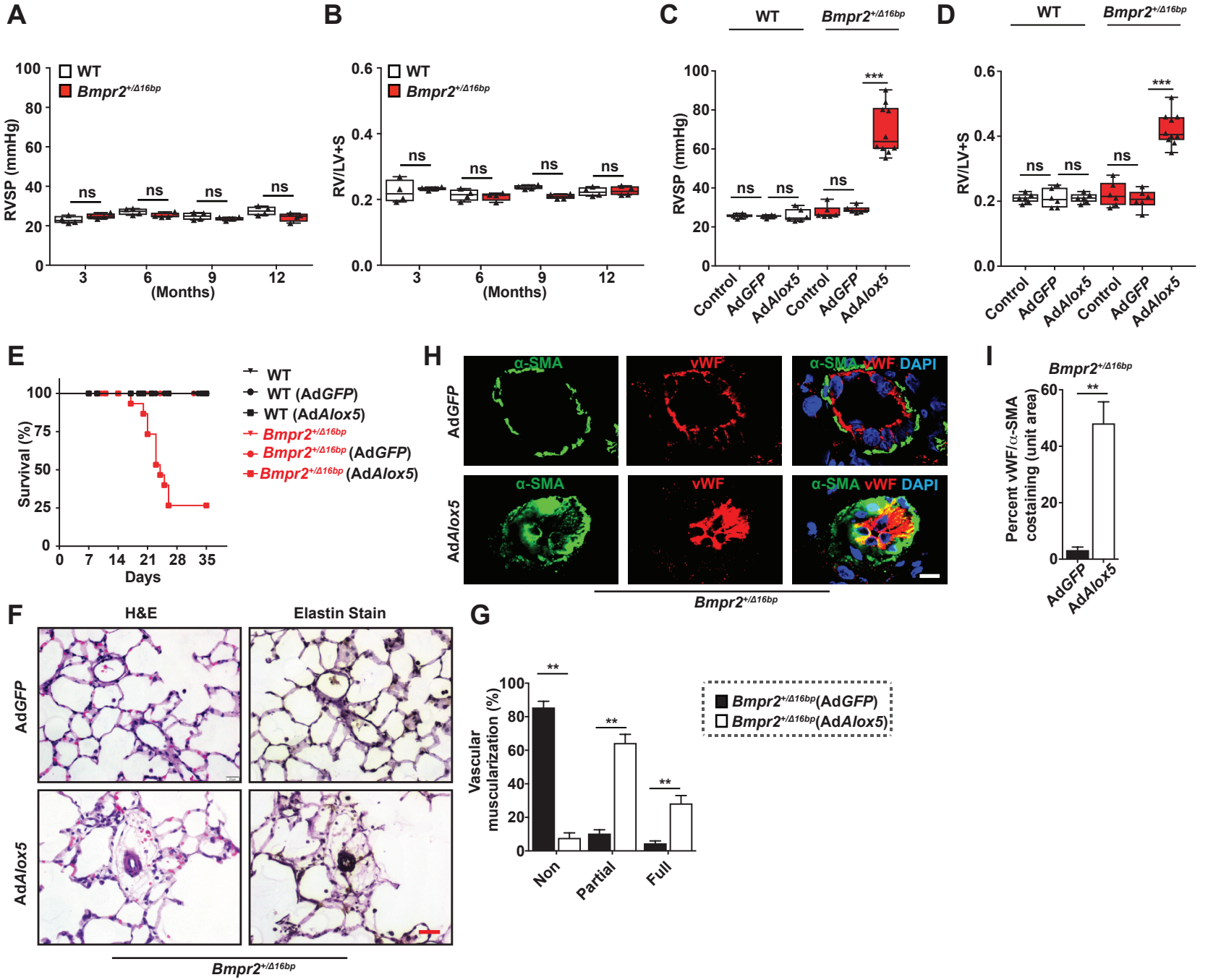

Supplemental Figure 5

Progressive inflammation induced by Ad*Alox5* causes PAH in the *Bmpr2*$^{+/\Delta 527bp}$ rats

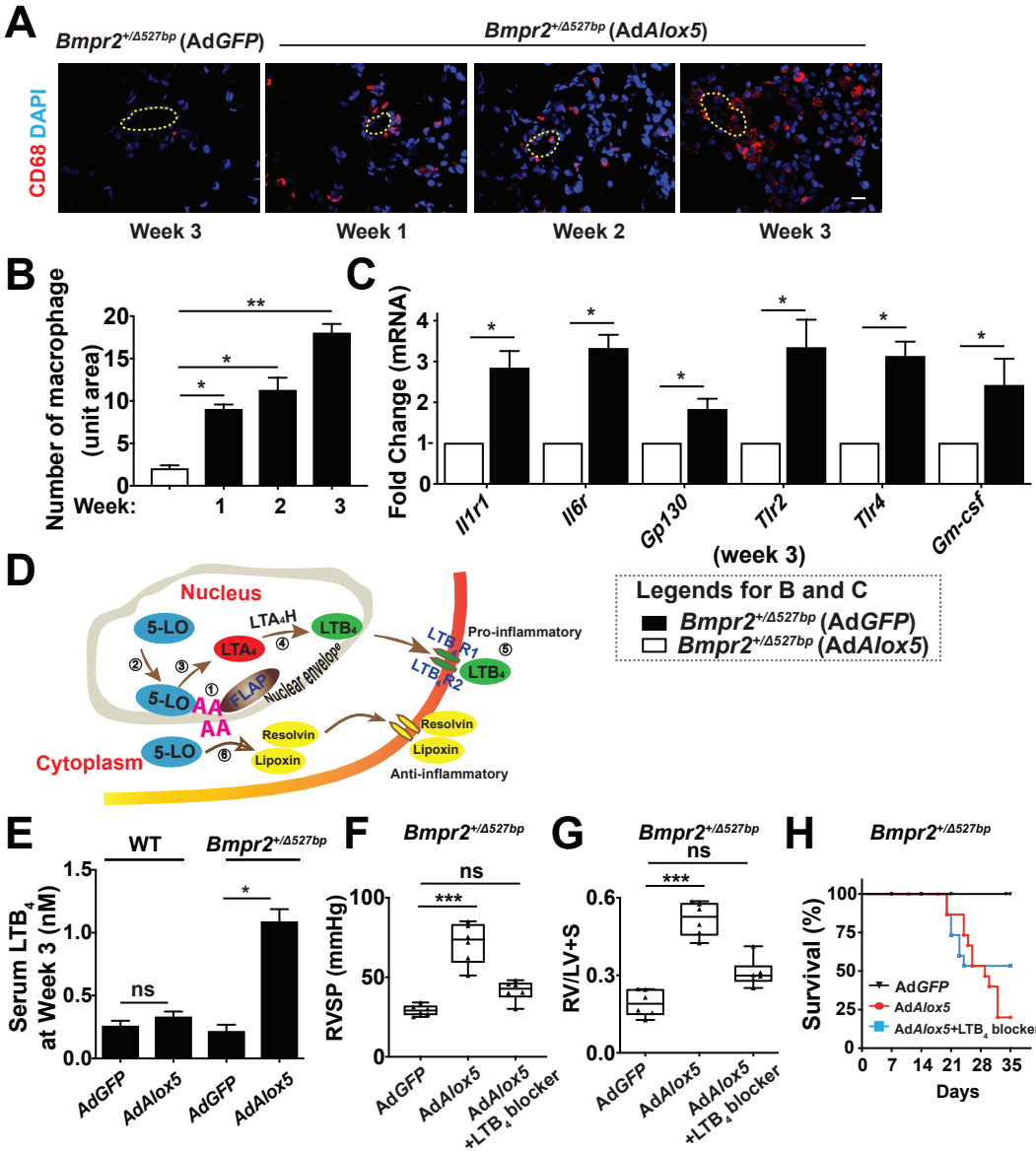

Supplemental Figure 6.

Ad*Alox5* infects airway epithelium and alveolar macrophages and recedes by week 2; in its place a 5-LO^{+} neointima emerges which is non-viral in origin and produces endogenous LTB_4

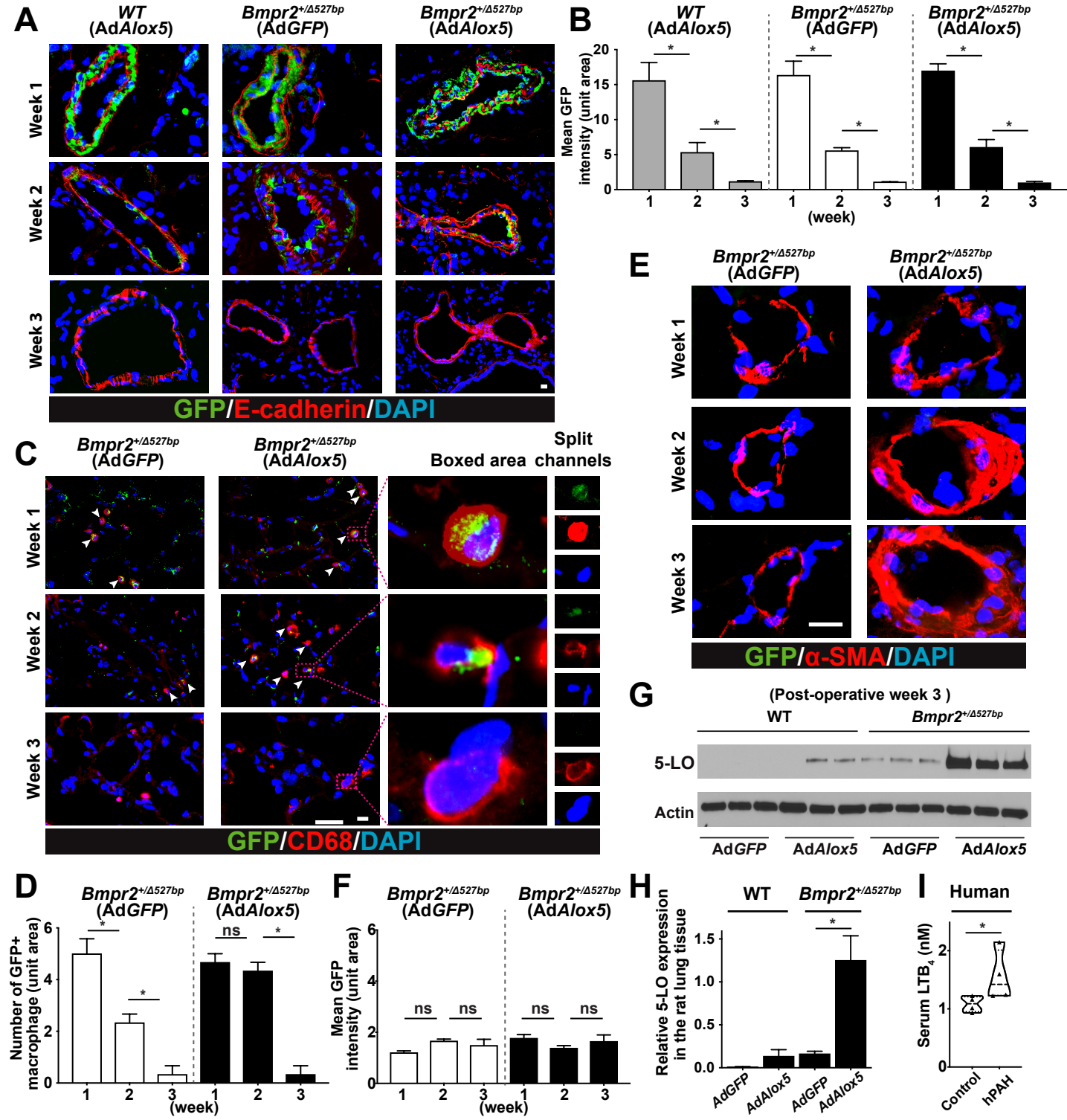

Supplemental Figure 7

PAECs with reduced BMPR2 and enhanced 5-LO display unique transcriptome profile similar to clinical samples

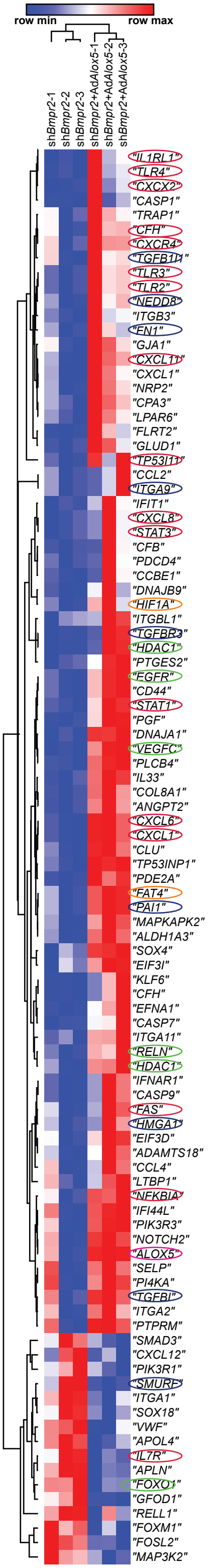

Supplemental Figure 8

LTB_4 diminishes BMPR2 signaling in PAECs with impaired *Bmpr2*

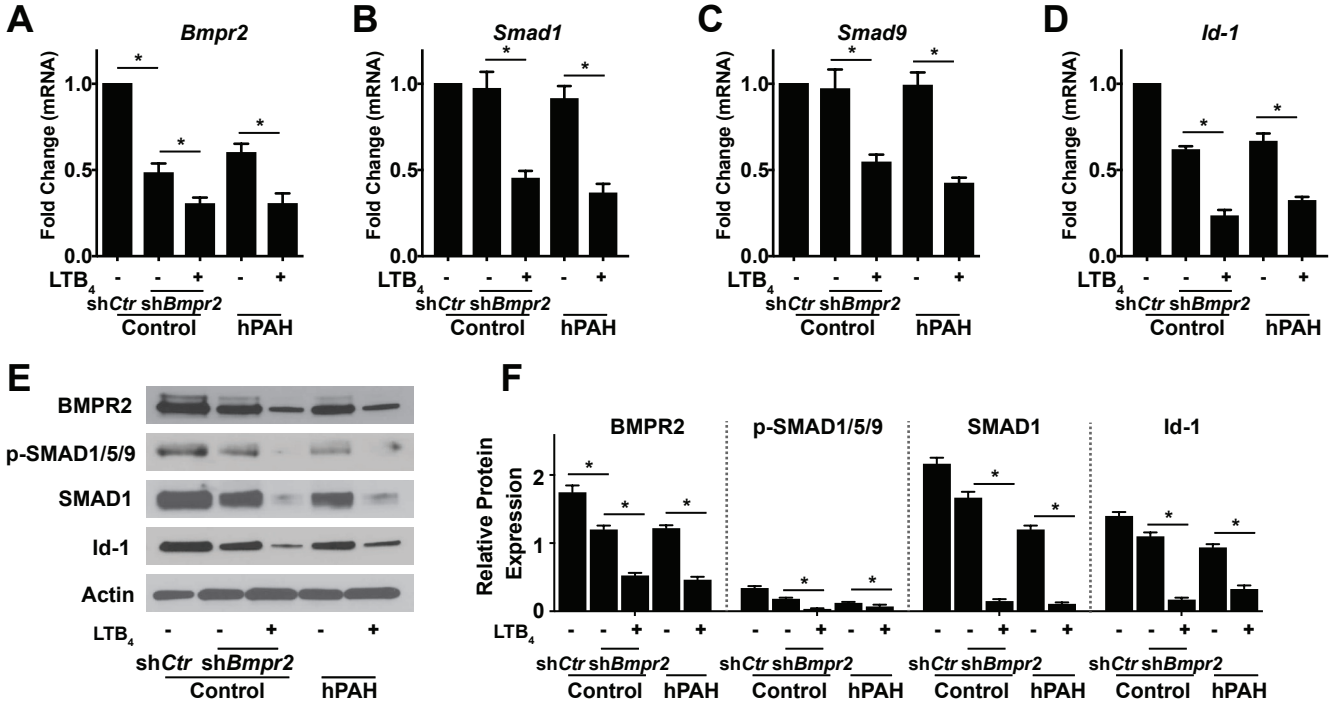

Supplemental Figure 9

BMPR2 insufficiency combined with increased LTB_4 induces PAEC transformation in a step-wise process : LTB_4-mediated apoptosis, apoptosis-resistant proliferation followed by EndMT

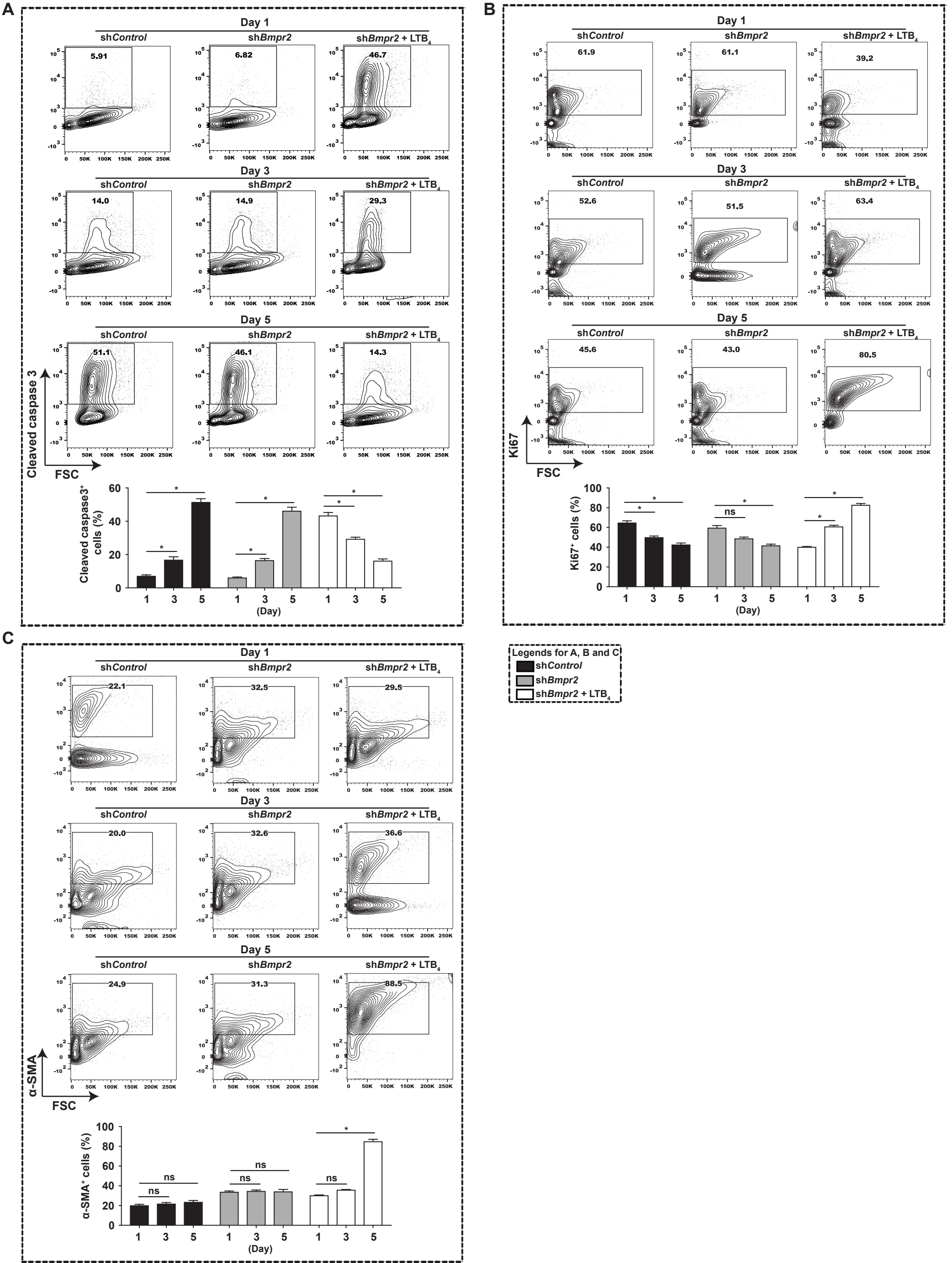

Supplemental Figure 10

LTB_4 induces proliferation of PAECs with reduced BMPR2 signaling

A

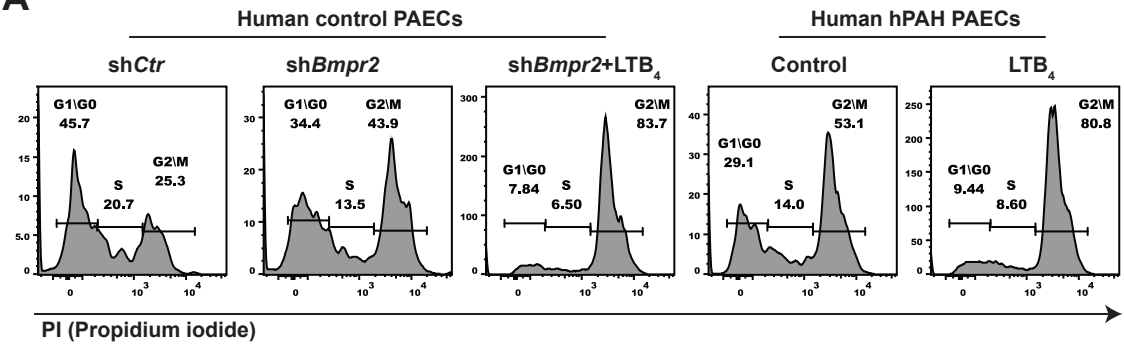

B

	G1/G0	S	G2/M
Control sh*Ctr*	45.7	20.7	25.3
Control sh*Bmpr2*	34.4	13.5	43.9
Control sh*Bmpr2*+LTB_4	7.84	6.5	83.7
hPAH Control	29.1	14	53.1
hPAH LTB_4	9.44	8.6	80.8

Supplemental Figure 11

Blocking canonical or noncanonical TGF-β signaling inhibits LTB_4-induced TGF-β activation in PAECs with low BMPR2 expression

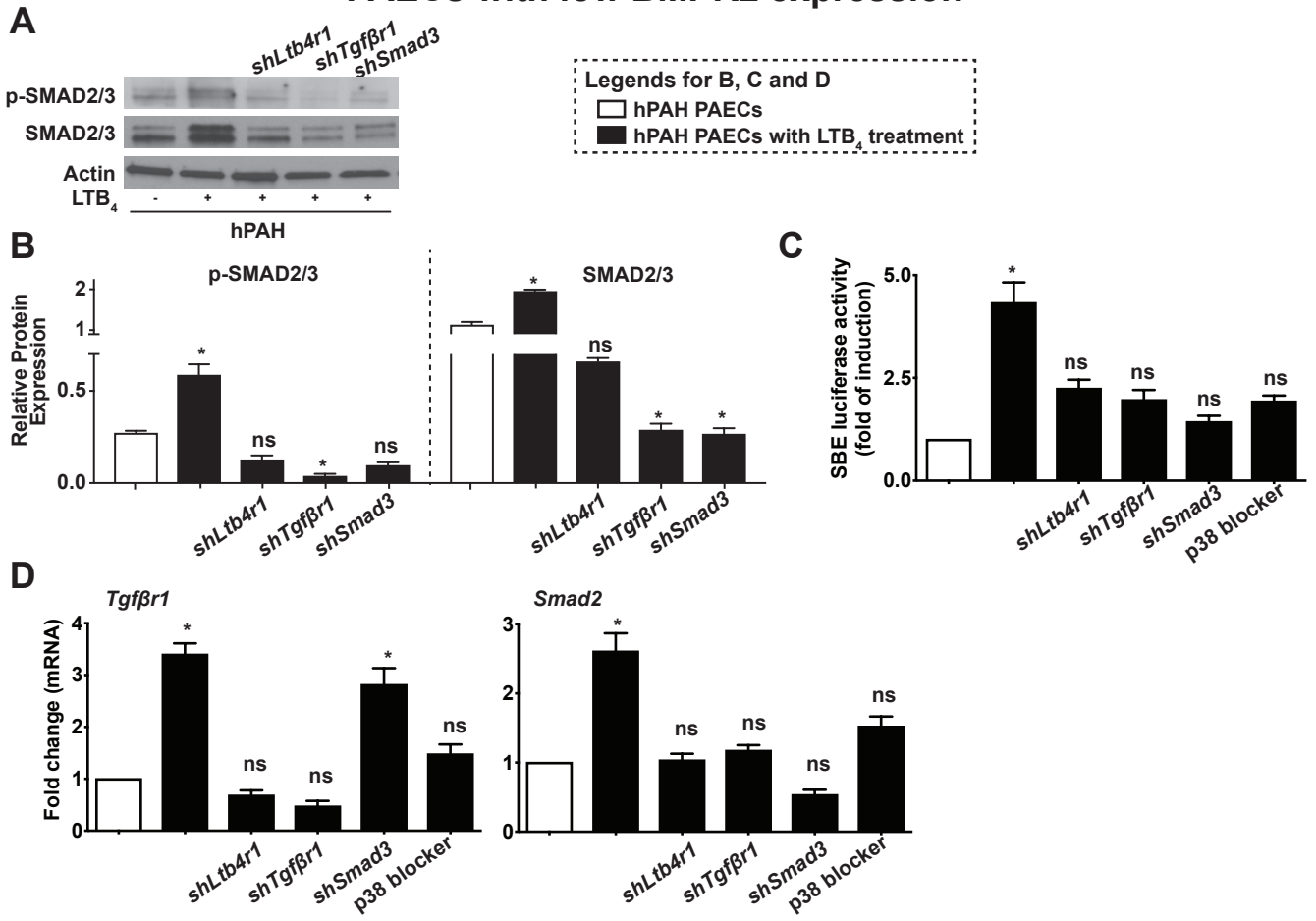

Supplemental Figure 12

Impaired BMPR2 signaling combined with LTB_4 induces a step-wise PAEC transformation: a p38-mediated noncanonical TGFβ-dependent proliferation followed by a canonical TGFβ-mediated EndMT

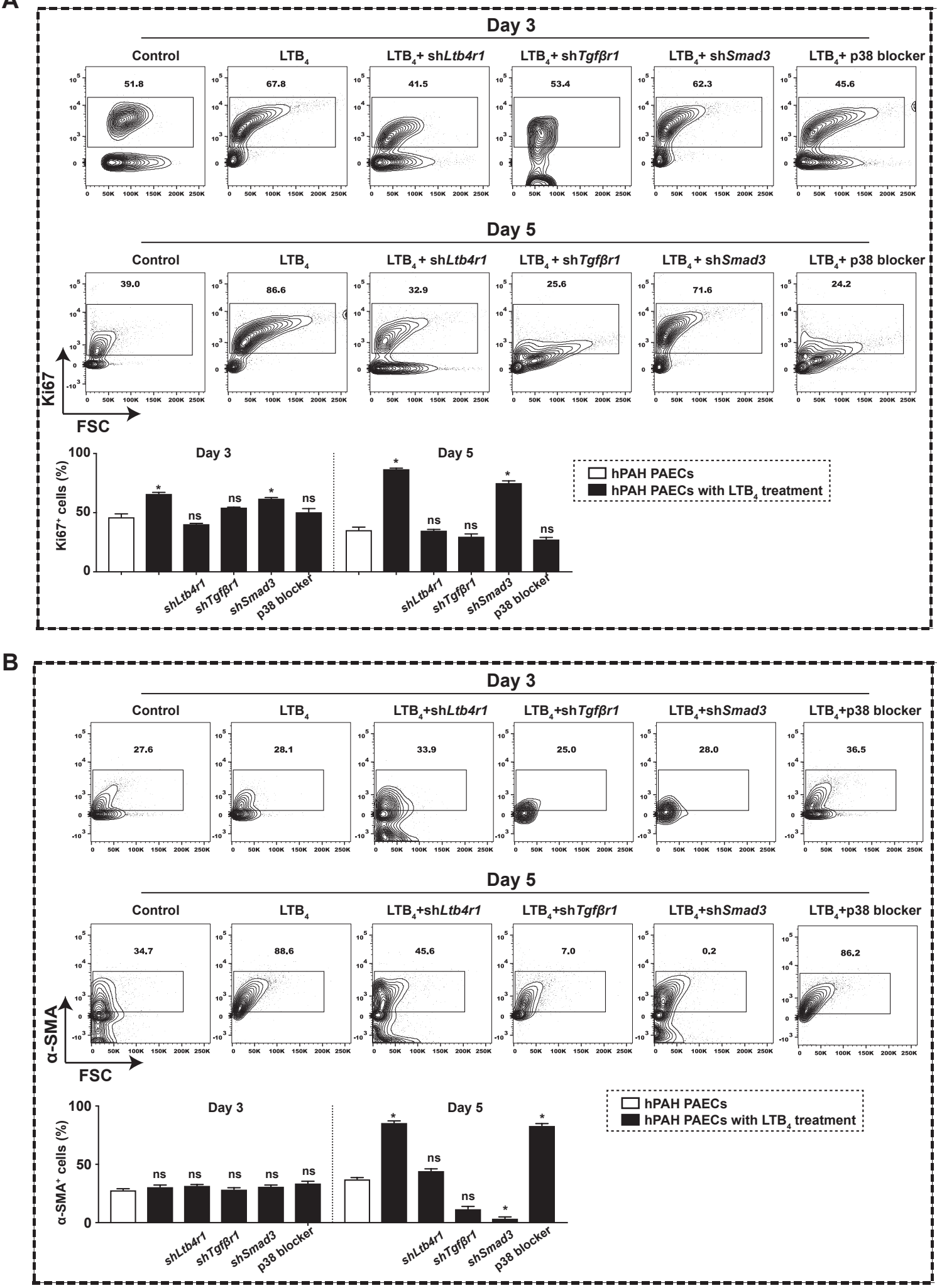

Supplemental Figure 13

Blocking p38-mediated noncanonical TGF-β signaling reverses LTB_4-induced PAEC proliferation

A

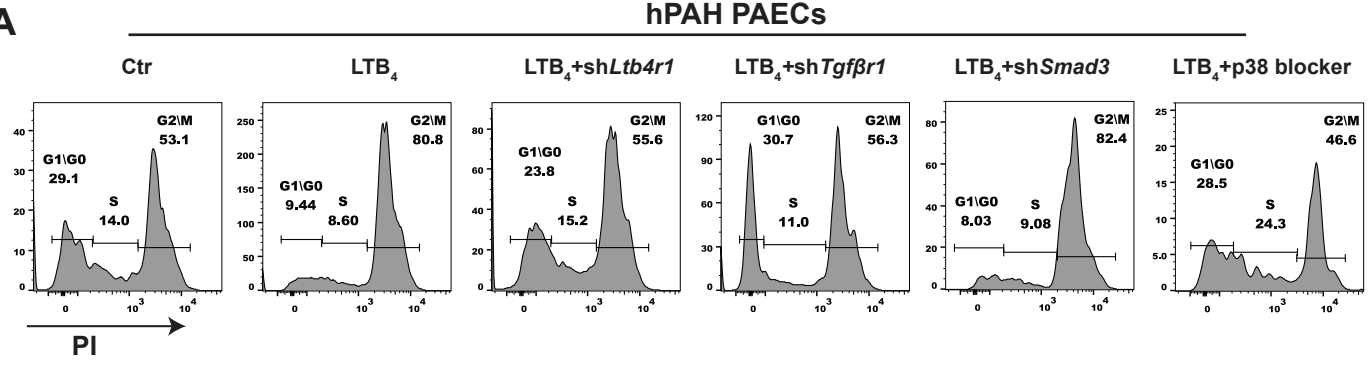

B

	G1/G0	S	G2/M
ctr	29.1	14	53.1
LTB_4	9.44	8.6	80.8
LTB_4+sh*Ltb4r1*	23.8	15.2	55.6
LTB_4+sh*Tgfβr1*	30.7	11	56.3
LTB_4+sh*Smad3*	8.03	9.08	82.4
LTB_4+p38 blocker	28.5	24.3	46.6

Supplemental Figure 14

Blocking canonical TGF-β signaling reverses LTB_4-induced PAEC EndMT

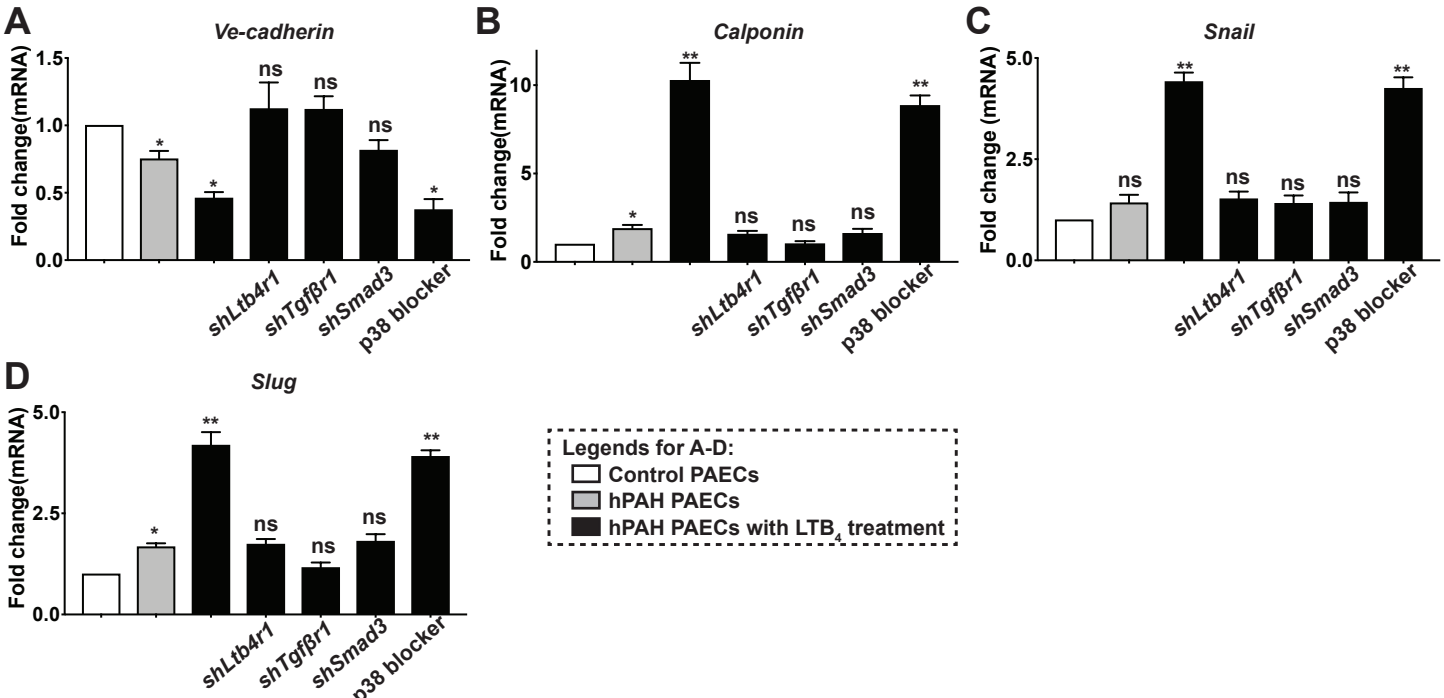

Supplemental Figure Legends:

Supplemental Figure 1. Generation of the *Bmpr2*$^{+/\Delta 527bp}$ and the *Bmpr2*$^{+/\Delta 16bp}$ rats using Zinc Finger Nuclease technology. Zinc Finger Nuclease technology was used to introduce a reading frame shift in the *Bmpr2* gene. Schematic overview of *Bmpr2* gene with WT and mutant alleles. *Bmpr2* mutant rats with a monoallelic deletion of 527bp (Δ527 crosses intron and exon1 boundary) or 16bp (Δ16 in exon1) were generated.

Supplemental Figure 2. Ad*Alox5* induces severe PAH in the *Bmpr2*$^{+/\Delta 527bp}$ rats through LTB_4 signaling. (**A** and **B**) Weekly hemodynamic assessments of WT and *Bmpr2*$^{+/\Delta 527bp}$ rats exposed to Ad*Alox5* or GFP-tagged control vector, Ad*GFP*. (**C** and **D**) Weekly echocardiographic analysis measures the right ventricular (RV) free wall thickness and pulmonary artery (PA) acceleration time. (**E**) Hemodynamics of left ventricle assessed by left heart catheterization. For panels **A** and **B**, data are presented in box-and-whiskers plots showing minimal to maximal values and all data points; for panel **D**, data are presented as mean and SEM; Kruskal-Wallis test; ns, not significant, *p< 0.05, **p < 0.01, ***p<0.001.

Supplemental Figure 3. *Bmpr2*$^{+/\Delta 527bp}$ and WT rats respond similarly to MCT, SU5416 or chronic hypoxia. Hemodynamic measurements of WT and *Bmpr2*$^{+/\Delta 527bp}$ rats after a single dose of monocrotaline (MCT, 60mg/kg; **A** and **B**), () a single dose of SU5416 (20mg/kg; **C** and **D**) at post-treatment week 3. Alternatively, rats were exposed to 10% O_2 for 3 weeks without (**E** and **F**) or with SU5416 administration (**G** and **H**). All data are presented in box-and-whiskers plots showing minimal to maximal values and all data points; for panel **A**-**D**, Kruskal-Wallis test, for panels **E**-**H**, Mann-Whitney test; ns, not significant, *p< 0.05, ***p<0.001.

Supplemental Figure 4. Ad*Alox5* induces severe PAH in the *Bmpr2*$^{+/16bp}$ rats. (**A** and **B**) Assessments of RVSP (**A**) and RV/LV+S (**B**) of the *Bmpr2*$^{+/\Delta 16bp}$ rats at the 3, 6, 9 or 12 months of age. Hemodynamics measurements of WT cohort in the same age groups were analyzed in parallel. (**C**-**E**) Assessments of RVSP (**C**), RV/LV+S (**D**) and percentage of survival (**E**) of WT or *Bmpr2*$^{+/\Delta 16bp}$ rats receiving intratracheal instillation of Ad*Alox5* or Ad*GFP*. Rats not subjected to virus treatment were used as controls. Hemodynamics measurements were performed at post-operative week 3. Female and male rats were randomly assigned to different experimental groups. (**F** and **G**) Representative hematoxylin and eosin (H&E) and Elastin stain images and quantification of percentage vascular muscularization. n=6; scale bar, 100μm. (**H** and **I**) Representative images and quantification of α-SMA (green) and vWF (red) staining. DAPI (blue) identifies nuclei. n=6; scale bar, 50μm. For panels **A**-**D**, data are presented in box-and-whiskers plots showing minimal to maximal values and all data points; for panel **E**, data are presented by Kaplan-Meier survival plot; for panels **G** and **I**, data are presented as mean and SEM; for panels **A**, **B**, **G** and **I**, Mann-Whitney test; for panels **C** and **D**, Kruskal-Wallis test; ns, not significant, *p< 0.05, **p < 0.01, ***p<0.001.

Supplemental Figure 5. Progressive lung inflammation induced by AdAlox5 causes PAH in the *Bmpr2*$^{+/-}$ rats. (**A** and **B**) Representative images and quantification of $CD68^+$

macrophages (red). White dash lines outline the small distal PAs. DAPI stains the nuclear. n=6; scale bar, 50μm. (**C**) Quantification of whole lung transcripts of *Il1r1* (interleukin 1 receptor 1), *Il6r* (IL6 receptor), *gp130* (IL6 receptor subunit beta), *Tlr2* (Toll-like receptor 2), *Tlr4* and *Gm-csf* (granulocyte-macrophage colony stimulating factor) using Autoimmunity RT^2 Profiler PCR array kit. Tissues were collected at post-operative week 3. (**D**) Cartoon illustration of 5-LO signaling pathways for the synthesis of pro-inflammatory or anti-inflammatory eicosanoid lipids. 1) AA (arachidonic acid) is released from the phospholipid membrane. 2) Nucleoplasmic 5-LO translocates to the nuclear envelope and ER/Golgi membrane. 3) Facilitated by FLAP (5-LO activating protein), 5-LO converts inner nuclear envelope-localized AA to LTA_4 (leukotriene A_4). 4) LTA_4 is metabolized to LTB_4 by LTA_4H (LTA_4 hydrolase) in the nucleus. 5) Pro-inflammatory LTB_4 acts on target cell through binding to its cognate high-affinity receptor, LTB_4R1 (LTB_4 receptor 1, also named as BLT1), or low-affinity receptor, LTB_4R2 (LTB_4 receptor 2, BLT2). 6) Cytoplasmic 5-LO converts outer nuclear envelope-localized AA to anti-inflammatory resolvins and lipoxins. (**E**) ELISA measurements of blood serum LTB_4 collected at post-operative week 3. (**F-H**) *Bmpr2*$^{+/\Delta 527bp}$ rats were treated with a LTA_4H antagonist, bestatin (1mg/kg, oral, Q.D), for 2 weeks starting at week 3 following virus instillation. Hemodynamic assessments were performed at week 5. For panels **B** and **E**, data are presented as mean and SEM, Kruskal-Wallis test; for panel **C**, data are presented as mean and SEM, Mann-Whitney test; for panels **F** and **G**, data are presented in box-and-whiskers plots showing minimal to maximal values and all data points, Kruskal-Wallis test; for panel **H**, data are presented by Kaplan-Meier survival plot; ns, not significant, *p< 0.05, **p < 0.01, ***p<0.001.

Supplemental Figure 6. Ad*Alox5* infects airway epithelium and alveolar macrophages and recedes by week 2; it generates a 5-LO$^+$ neointima which is non-viral in origin and produces endogenous LTB_4. Lung sections from WT or *Bmpr2*$^{+/\Delta 527bp}$ rats exposed to Ad*Alox5* or Ad*GFP* were harvested weekly following viral instillation. (**A** and **B**) Representative images and quantification of fluorescent staining of GFP-tagged virus (GFP, green) and epithelium marker, E-Cadherin (red). Note both *Alox5* and *GFP* transgene were concentrated in the airway epithelium 1 week after infection and gradually receded in all animal groups. No measurable differences were seen in the transduction efficiency between two viral particles. n=6; scale bar, 50μm. (**C** and **D**) Representative images and quantification of GFP-tagged virus (green) and CD68$^+$ macrophages (red). Boxed area with split channels illustrates viral infection in alveolar macrophages. n=6; scale bar, 50μm. (**E** and **F**) Representative images and quantification of GFP-tagged virus (green) and vWF$^+$ PA endothelium. Note viral activities were not detectable in distal PAs. n=6; scale bar, 50μm. (**G** and **H**) Representative western blots and quantification of 5-LO in lung tissue collected 3 weeks after viral infection from WT and *Bmpr2*$^{+/\Delta 527bp}$ rats assigned in different treatment groups. Actin was used as loading control. n=3. (**I**) Blood serum LTB_4 measurements of 4 control subjects and 4 hPAH patients with *Bmpr2* mutations. For panels **B**, **D**, **F** and **H**, data are presented as means and SEM, Kruskal-Wallis test; for the panel **I**, data are presented as violin plots showing all data points, Mann-Whitney test; ns, not significant, *p< 0.05.

Supplemental Figure 7. PAECs with reduced BMPR2 and enhanced 5-LO display a unique transcriptome profile similar to clinical disease. Heatmap with hierarchical clustering indicating representative differentially expressed genes (DEGs) between sh*Bmpr2*+Ad*Alox5* (two-hit model) versus sh*Bmpr2* (one hit condition) treatment groups. Red circle features inflammatory genes; blue circle highlights genes implicated in EndMT; green circle highlights genes important for cell proliferation and orange one features genes responsible for cell metabolism.

Supplemental Figure 8. LTB_4 diminishes BMPR2 signaling in PAECs with impaired *Bmpr2* expression. To mimic BMPR2 signaling loss *in vitro*, PAECs from control donor were infected with sh*Bmpr2* expressing lentivirus or control virus (sh*Ctr*) and were compared with cells collected from hPAH patient bearing *Bmpr2* mutations. PAECs were subsequently cultured in 400nM LTB_4 or vehicle in the serum-free medium for 7 days to assess the effects of increased 5-LO-mediated inflammation. (**A-D**) qPCR analysis of mRNA transcription of *Bmpr2*, *Smad1*, *Smad9* and *Id-1*. (**E** and **F**) Representative western blots and quantification of BMPR2, p-SMAD1/5/9, SMAD1 and Id-1. Actin was used as the loading control. n=3. All data are presented as means and SEM; Kruskal-Wallis test; ns, not significant, *p< 0.05.

Supplemental Figure 9. BMPR2 insufficiency combined with increased LTB_4 induces PAEC transformation in a step-wise process: LTB_4-mediated apoptosis, apoptosis-resistant proliferation followed by EndMT. Control PAECs infected with control vector (sh*Control*) or sh*Bmpr2* were cultured with or without 400nM LTB_4 in the serum-free medium and were then assessed for cleaved Caspase 3, Ki67 and α-SMA expression on post-treatment day 1, 3 and 5. Representative flow cytometry contour plots and quantification were presented. n=6. All data are presented as means and SEM; Kruskal-Wallis test; ns, not significant, *p< 0.05.

Supplemental Figure 10. LTB_4 induces proliferation of PAECs with reduced BMPR2 signaling. (**A** and **B**) Representative flow cytometry histograms from propdium iodide-(PI) -mediated cell cycle analysis. Cell population under each of the G1/G0, S and G2/M phase was analyzed by Flowjo. n=6.

Supplemental Figure 11. Blocking canonical or noncanonical TGFβ signaling inhibits the LTB_4-induced TGFβ activation in PAECs with low BMPR2 expression. PAECs from hPAH patient were either infected with lentivirus of sh*Ltb4r1*(shRNA targeting LTB_4 receptor 1, LTB_4R1), sh*Tgfβr1* (shRNA silencing TGF-β receptor 1, TGFβR1), sh*Smad3*, or were treated with a p38 blocker (SB203580, 1uM). All measurements were carried out 7 days post-treatment. (**A** and **B**) Representative western blots and quantification of p-SMAD2/3 and SMAD2/3. Actin was used as loading control. n=3. (**C**) SBE (SMAD binding element)-mediated reporter assays. n=6. (**D**) qPCR analysis of mRNA transcription of *Tgfβr1* and *Smad2.* n=6. All data are presented as means and SEM; Kruskal-Wallis test between treatment groups versus the control groups (white bar); ns, not significant, *p< 0.05.

Supplemental Figure 12. Impaired BMPR2 signaling combined with LTB_4 induces a

step-wise PAEC transformation: a p38-mediated noncanonical TGFβ-dependent proliferation followed by a canonical TGFβ-mediated EndMT. PAECs from hPAH patient were assessed for Ki67 and α-SMA expression on posttreatment day 3 and day 5 by flow cytometry. n=6. All data are presented as means and SEM; Kruskal-Wallis test between treatment group versus the control group (white bar); ns, not significant, *p< 0.05.

Supplemental Figure 13. Blocking p38-mediated noncanonical TGF-β signaling reverses LTB_4-induced PAEC proliferation. PAECs from hPAH patient were either infected with lentivirus of sh*Ltb4r1*, sh*Tgfbr1*, sh*Smad3* or were treated with a p38 blocker (SB203580,1uM) for 7 days. These cells were then subjected to PI-mediated cell cycle analysis (**A** and **B**). n=6.

Supplemental Figure 14. Blocking canonical TGF-β signaling reverses LTB_4-induced PAEC EndMT. PAECs from hPAH patients were subjected to qPCR analysis of mRNA transcription of *Ve-cadherin* (marker of endothelial tight junction), *Calponin* (marker of mesenchymal cell), *Snail* and *Slug* ((critical transcriptional factors for endothelium to mesenchymal transition (EndMT)). n=6. All data are presented as means and SEM; Kruskal-Wallis test between treatment groups versus the control groups (white bar); ns, not significant, *p< 0.05, **p< 0.01.